43rd IEEE International Conference on Plasma Science,
June 19-23, 2016

Submission of the papers to a regular issue of the IEEE Transactions on Plasma Science

Sunday, 19 June 2016	Monday, 20 June 2016	Tuesday, 21 June 2016	Wednesday, 22 June 2016	Thursday, 23 June 2016	Friday, 24 June 2016
	0830 - 0930: Morning Plenary				**MINICOURSE 1 (9-12 AM and 2-5 PM):** Low-Power Atmospheric Pressure Plasma Sources (KCC 301) **MINICOURSE 2 (9:00am-12:30pm and 2-6 PM):** Plasma Simulation (KCC 303)
	Eric Harvey Theatre (PL1) Speaker: Riccardo Betti	**Eric Harvey Theatre (PL3)** Speaker: Graeme Lister	**Eric Harvey Theatre (PL5)** Speaker: James Irby	**Max Bell Auditorium (PL7)** Speaker: Gerard van Rooij	
	0930 - 1000: Coffee Break				
	1000 - 1230 Morning Orals				
	KCC 201 (1A): 7.4 Compact Pulsed Power and Application	**KCC 201 (3A):** 1.1 Basic Phenomena I	**KCC 201 (5A):** 1.2 Computational Plasma Physics I	**KCC 101 (7A):** 1.2 Computational Plasma Physics II	
	KCC 203 (1B): 2.1 Intense Beam Microwave Generation / 2.2 Fast Wave Devices	**KCC 203 (3B):** 2.7 Special Session - Microwave Generated Plasmas on Spacecraft	**KCC 203 (5B):** 2.4 Vacuum Microelectronics / 2.6 Non-Fusion Microwave Systems / 2.8 THz Sources	**KCC 103 (7B):** 2.3 Slow-Wave Devices	
	KCC 205 (1C): 5.1 Nonequilibrium Plasma Applications I	**KCC 205 (3C):** 4.6 Fast Z pinches II	**KCC 205 (5C):** 4.5 Laser Produced Plasmas	**KCC 105 (7C):** 1.4 Partially Ionized Plasmas II / 1.6 Plasma Chemistry II	
	KCC 301(1D): 4.1 Fusion (Inertial, Magnetic and Alternate Concepts)	**KCC 301(3D):** 4.2 Particle Acceleration with Laser and Beams	**KCC 301(5D):** 4.3 Special Session on Shiva Star	**KCC 301(7D):** 4.6 Fast Z-Pinches III	
	KCC 303 (1E): 5.3 Plasma Thrusters	**KCC 303 (3E):** 5.5 Environmental and Industrial Applications	**KCC 303 (5E):** 1.6 Plasma Chemistry I	**KCC 303 (7E):** 5.2 High-Pressure and Thermal Plasma Processing	
	KCC 305 (1F): 6.2 Particle Diagnostics / 6.1 Optical and X-ray Diagnostics I	**KCC 305 (3F):** 6.3 Electrical (Probe) Diagnostics / 6.1 Optical, FIR and Microwave Diagnostics II	**KCC 305 (5F):** 6.1 Optical, X-ray, FIR and Microwave Diagnostics III	**KCC 305 (7F):** 7.2 Opening and Closing Switches / 7.3 Generators and Applications	
	1200 - 1330: LUNCH			**CONFERENCE END**	
	1330 - 1430: Afternoon Plenary			**MINICOURSE 1 (2-6 PM):** Low-Power Atmospheric Pressure Plasma Sources (KCC 301) **MINICOURSE 2 (2-5 PM):** Plasma Simulation (KCC 303)	
	Eric Harvey Theatre (PL2) Speaker: David Knudsen	**Eric Harvey Theatre (PL4)** Speaker: Christine Coverdale (2016 PSAC Award Winner)	**Eric Harvey Theatre (PL6)** Speaker: Mark Kushner (2015 Birdsall Award Winner)		
1400 - 1800: Registration Begins (Kinnear Centre Lobby)	**1430 - 1600: Posters Session (43W x 45H inches) KCC 101, 103, 105 (1P)** 1.1, 1.3, 1.6, 2.1, 2.2, 2.3, 3.1, 4.1, 4.4, 5.1, 5.2, 5.3, 5.5, 7.1, 7.2	**1430 - 1600: Posters Session (43W x 45H inches) KCC 101, 103, 105 (1P)** 1.1, 1.2, 1.4, 2.4, 2.5, 3.2, 4.1, 4.5, 4.6, 5.2, 5.4, 5.6, 6.1, 7.3	**1430 - 1600: Posters Session (43W x 45H inches) KCC 101, 103, 105 (1P)** 1.2, 1.5, 1.6, 2.6, 2.7, 2.8, 4.2, 4.3, 4.5, 4.7, 5.1, 5.5, 5.6, 6.3, 7.4		
	1600 - 1830 Afternoon Orals	1600 - 1830 Afternoon Orals	1600 - 1800 Afternoon Orals		
	KCC 201 (2A): 1.3 Space Plasmas / 1.5 Dusty and Strongly Coupled Plasmas	**KCC 201 (4A):** 3.2 Intense Electron Ion Beams	**KCC 201 (6A):** 1.1 Basic Phenomena II		
	KCC 203 (2B): 2.5 Codes and Modeling I	**KCC 203 (4B):** 2.5 Codes and Modeling II	**KCC 203 (6B):** 2.7 Microwave Plasma Interaction		
	KCC 205 (2C): 3.1 Plasma, Ion and Electron Sources	**KCC 205 (4C):** 5.4 Plasmas for Lighting and Flat-Panel Displays	**KCC 205 (6C):** 1.4 Partially Ionized Plasmas I		
	KCC 301(2D): 4.7 Plasma Material Interactions	**KCC 301(4D):** 4.4 High Energy Density Matter I	**KCC 301(6D):** 4.3 Radiation Physics, X-ray Lasers / 4.4 High Energy Density Matter II		
	KCC 303 (2E): 4.6 Fast Z pinches I	**KCC 303 (4E):** 7.1 Insulation and Dielectric Breakdown	**KCC 303 (6E):** 2.5 Special Session - RF Breakdown and Multipactor		
	KCC 305 (2F): 5.6 Medical and Biological Applications I	**KCC 305 (4F):** 5.6 Medical and Biological Applications II	**KCC 305 (6F):** 5.1 Nonequilibrium Plasma Applications II		
	1830 - 2000: Women in Science & Engineering (ticket required) (Max Bell - Elder Tom Cran Room)	**18:30 - 20:00 Student and Young Professional Session (posters 43W x 45H inches) (Max Bell - Elder Tom Cran Room)**	**1800 - 1900: IEEE Plasma Sciences & Applications Committee, General Business Meeting (KCC 203, open to all)**		
1800 - 2000: Welcome Reception (Kinner Centre Quad Area and KCC 10,103,105)			**19:30 - 21:30 Awards Banquet (ticket required) (KCC 101,103,105)**		

OTHER EVENTS:	
Speaker Ready Room (KCC208)	all week
Interview Room (KCC 308)	all week

Electrode’s phenomena

Jaiwei Wu, Xi'an, Chine
Light emission and spectroscopy characteristics of an unconventional gas spark switch

PRES disponible

Study: An experimental investigation on degradation performance and decomposition behavior of polytetrafluoroethylen insulator materials

Why : increase the probability of flashover, reducing lifetime, stability and reliability

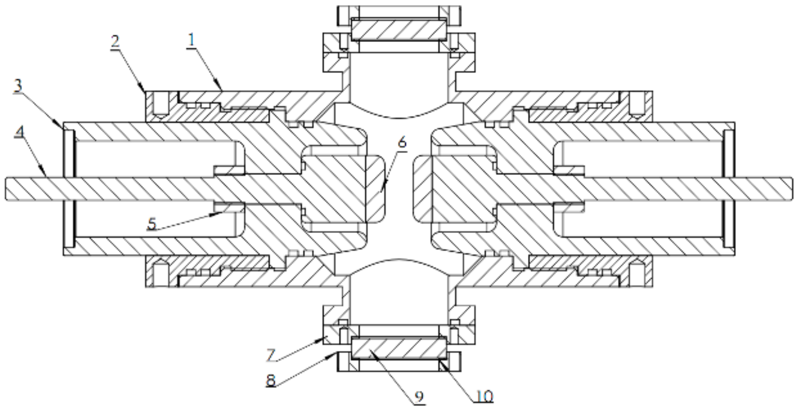

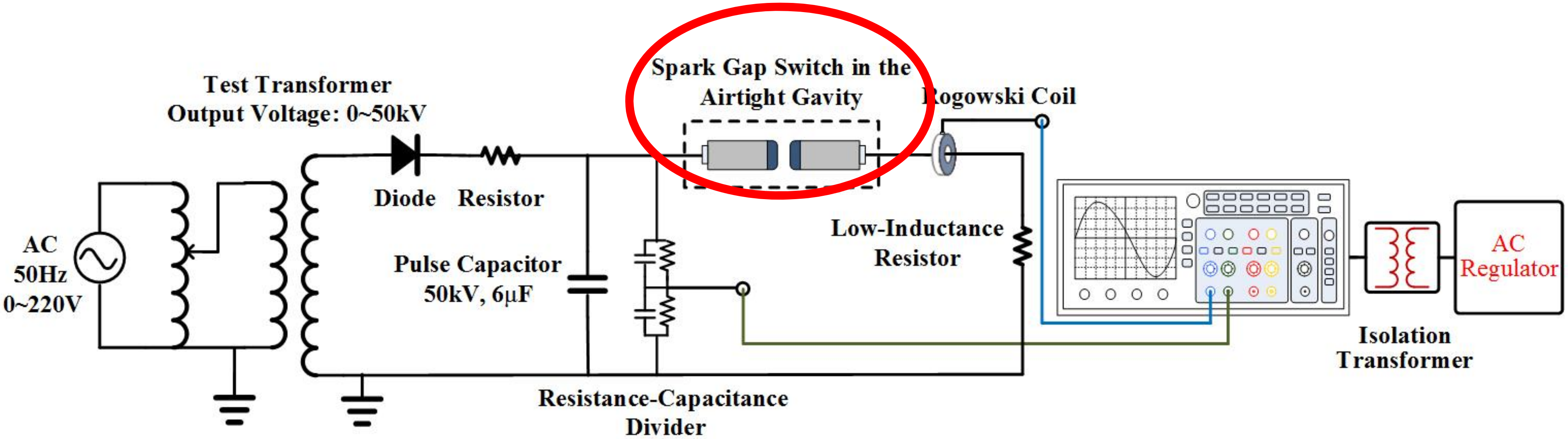

Jaiwei Wu, Xi'an, Chine

Light emission and spectroscopy characteristics of an unconventional gas spark switch

What :

Large Current Capacity | **Long Lifetime** | **High Self-breakdown voltage stability** | **Repetitive Operation**

Electrode Erosion | **Insulator Degradation Performance**

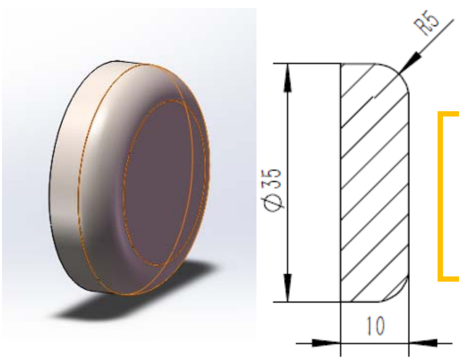

Electrode Material

Alloy Cu-W

90% mass percent of W

Discharge Parameters

- Peak self-breakdown voltage: **30 kV**
- Peak current : **57.5 kA**
- Repetitive rate : **0.1Hz**
- Transfer charge in one shot**: 0.883 C**
- Oscillation period : **20 µs**
- Pulse duration : **70 µs**
- One bar pressure of dry air

Methods :

X-ray induced photoelectron spectroscopy (XPS), every 5000 shots (to 20000 shots)

Gas chromatography AGILENT 7890A over 10000 shots

An Dynamic 3-D aspheric profiler Talysurf PGI 3D for surface roughness

Jaiwei Wu, Xi'an, Chine

Light emission and spectroscopy characteristics of an unconventional gas spark switch

Surface Anode

An Dynamic 3-D Aspheric Profiler
Talysurf PGI 3D

Surface Cathode


(a) Anode after 0 shots


(c) Anode after 10000 shots


(e) Anode after 20000 shots


(f) Cathode after 0 shots


(h) Cathode after 10000 shots

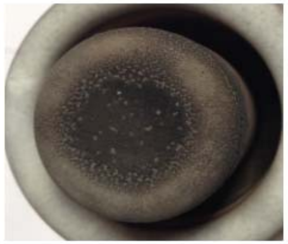
(j) Cathode after 20000 shots

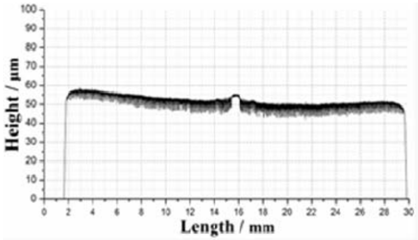

(a) Anode **after 0 shot**

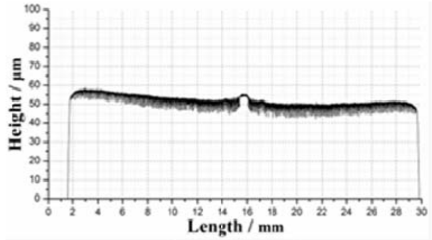

(b) Cathode after 0 shot

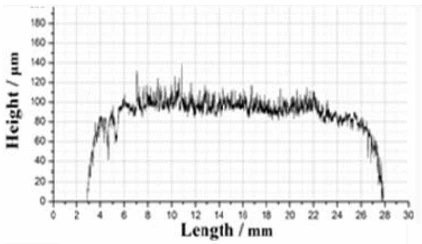

(e) Anode after 10000 shots

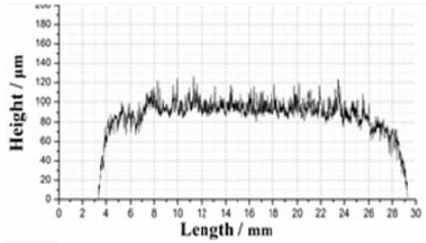

(f) Cathode after 10000 shots

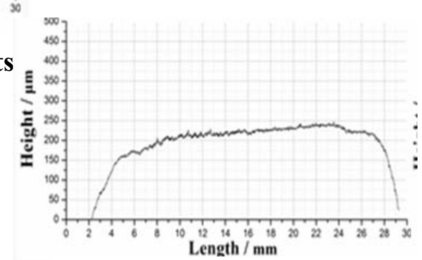

(i) Anode after 20000 shots

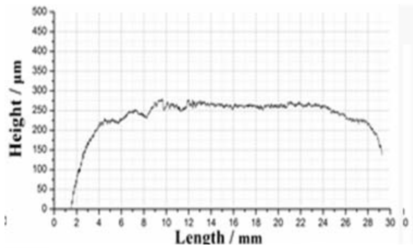

(j) Cathode after 20000 shots

Jaiwei Wu, Xi'an, Chine

Light emission and spectroscopy characteristics of an unconventional gas spark switch

Insulators Erosion Conditions

Polytetrafluoroethylene (PTFE)

-[-CF2-CF2-]n-

Thermal stability

Mechanical properties

Electrical insulation performance

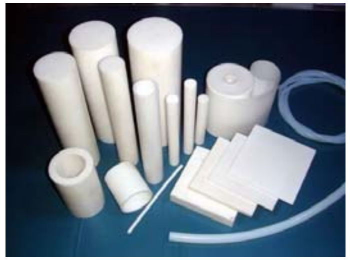

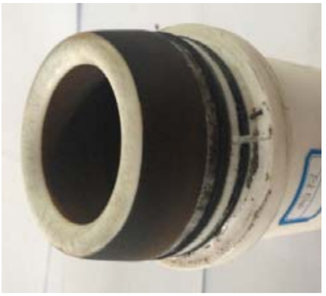

(a) Anode after 5600 shots

(d) Anode after 10000 shots

(c) Anode after 15000 shots

(d) Anode after 20000 shots

Cathode electrode showed a worse erosion surface.

(e) Cathode after 5600 shots

(f) Cathode after 10000 shots

(g) Cathode after 15000 shots

(h) Cathode after 20000 shots

Jaiwei Wu, Xi'an, Chine

Light emission and spectroscopy characteristics of an unconventional gas spark switch

Degradation Performance | **Polytetrafluoroethylene (PTFE)** | **Solid Products**

X Ray Photoelectron Spectroscopy (XPS) Axis Ultra DLD-600W
Anode and Cathode Insulators Surfaces after 10000 Shots

Element	Percentage of Atoms (%)				
	PTFE Material	Anode Insulator after 10000 Shots		Cathode Insulator after 10000 Shots	
		Inside Surface	Outside Surface	Inside Surface	Outside Surface
O	2.21	14.44	15.39	14.65	13.18
C	31.22	48.58	66.09	44.23	65.16
F	51.09	10.89	3.58	10.17	4.05
Ni	1.62	0.35	0.05	0.24	0.07
Si	3.97	1.89	1.01	2.32	2.50
W	/	1.10	0.84	1.01	0.54
Cu	0.23	0.51	0.13	0.68	0.08
K	7.86	/	/	/	4.87
Fe	/	0.44	0.13	0.29	/
Al	/	11.40	7.34	18.25	4.00
Ar	/	5.71	4.53	5.40	2.87
Ir	1.70	0.39	/	0.25	1.05
Mg	/	1.70	/	/	/
Tc	/	1.08	0.84	0.88	0.51
Cr	/	0.72	/	0.97	0.18
Cl	/	0.57	/	0.35	/
Pr	0.10	0.23	0.06	0.31	0.04

(1). Outside surface of insulator.

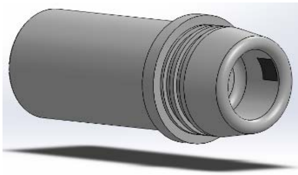

(2). Inside surface of insulator

10000 shots.

Atoms C left the surface. F reduced on the PTFE surfaces, ratio C/F increases shot after shot.

Jaiwei Wu, Xi'an, Chine

Light emission and spectroscopy characteristics of an unconventional gas spark switch

Degradation Performance | **Polytetrafluoroethylene (PTFE)** | **Gaseous Erosion**

Gas Chromatography (GC) AGILENT 7890A

Detectable Gas Species	Relative Content of Gaseous Products After 10000 shots	Relative Content of Gaseous Products After 20000 shots
Carbon Dioxide CO_2	100.0	100.00
Oxygen O_2	50.55	60.36
Carbon monoxide CO	7.85	12.66
Carbon Tetrafluoride CF_4	1.12	0.14
Nitrogen N_2	5.42	/
Hydrogen H_2	/	0.40

CO2, CO and CF4 gaseous product. Problem with CF4: electronegativity

D. Burkat, Canada

High-speed imaging and electrical diagnostocis of interacting arcs in dual cathode electric arc furnace

PRES disponible

Application : arc furnaces(EAF), solid waste gasification, resource recovery (NRj, materials)
Goal: see if it's possible to distinguish merged arc and separate arcs using signal analysis.
Case : dual-cathode configuration with 2 individual arc with common anode

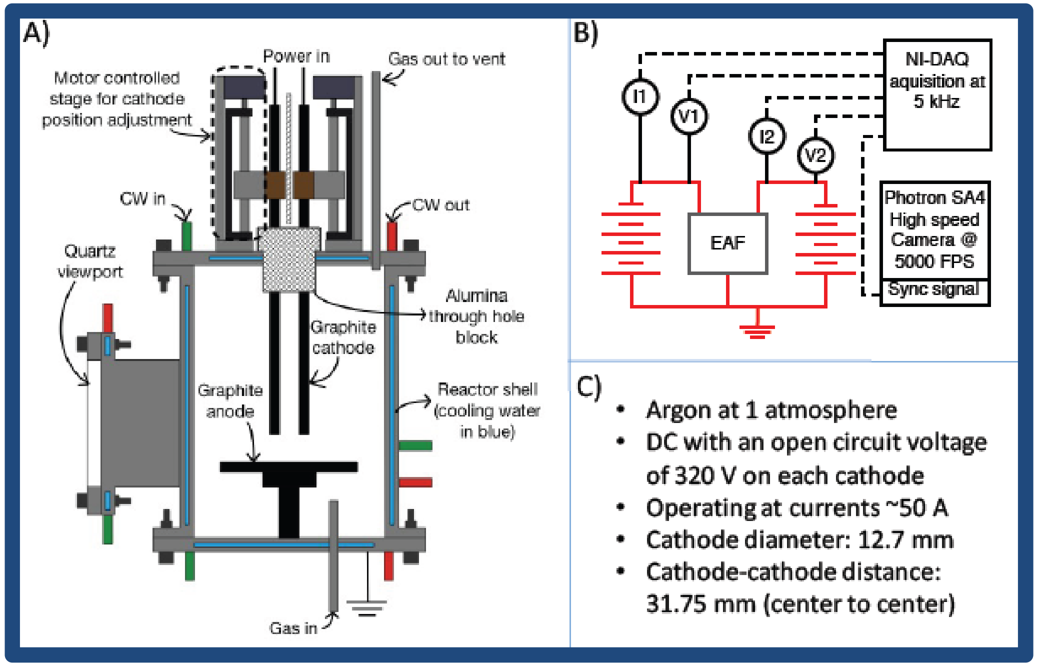

50A, 1 atm, Argon, graphite electrodes (ϕ=12.7mm, d=31.75mm)
Record of (V/I) characteristics in DC EAF, 5kHz synchro acquisition for V and I
High speed imaging for the arc's dynamics and correlation with (V,I)
Measure of arc's length, identify the structure

<u>Tools :</u> Model investigation with machine learning (artificial intelligence)

The raw data was separated into windows of 500 consecutive frames along with the 500 corresponding voltage and current values (total of 917 windows).

The MATLAB® Statistics and Machine Learning Toolbox was used to find a useful model relating the arc structures with the electrical signals (Dijkstra's path algorithm to reconstruct the path of highest brightness between anode and cathode). Two kinds of variables are necessary to train a model with machine learning: predictor and response variables.

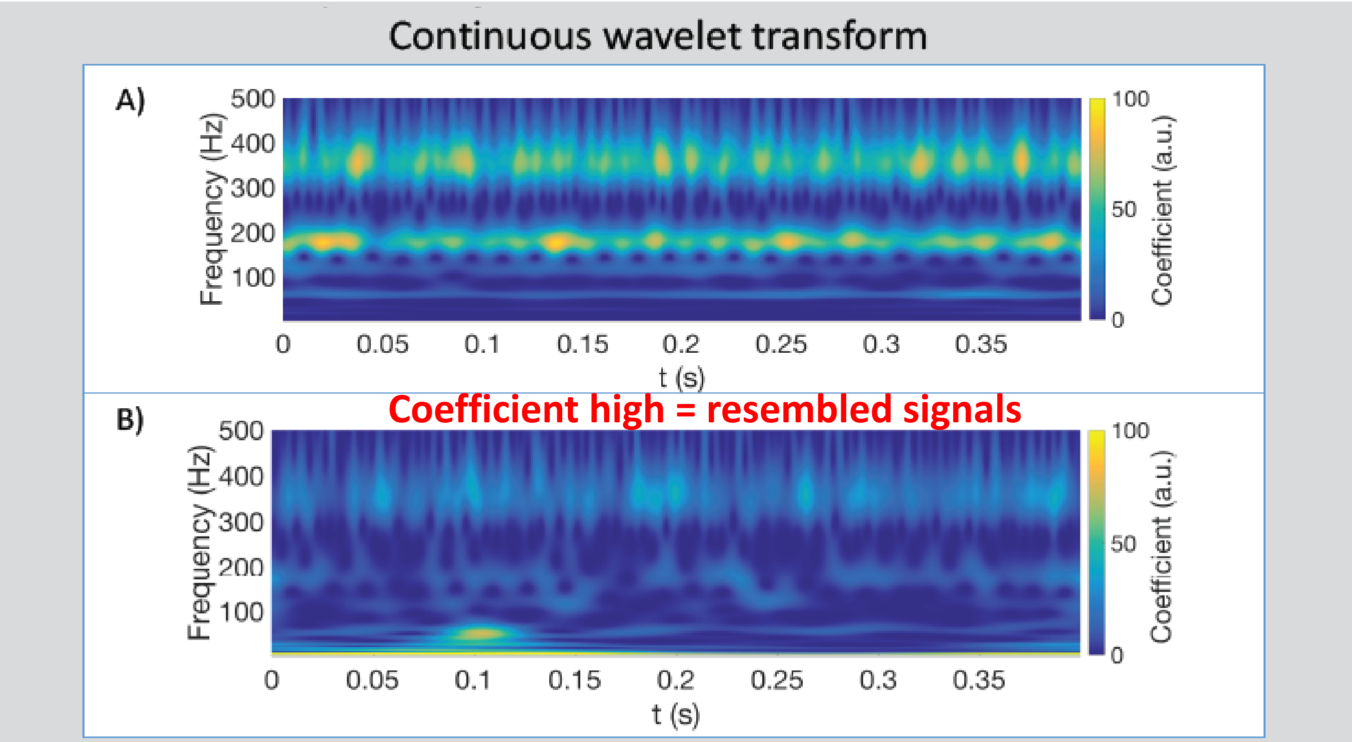

Use of MATLAB Wavelet Toolbox to obtain the Continuous waveler transform of current and voltage.

(A) Cathode and anode contact (no arc)

(B) Separate arc

D. Burkat, Canada

High-speed imaging and electrical diagnostics of interacting arcs in dual cathode electric arc furnace

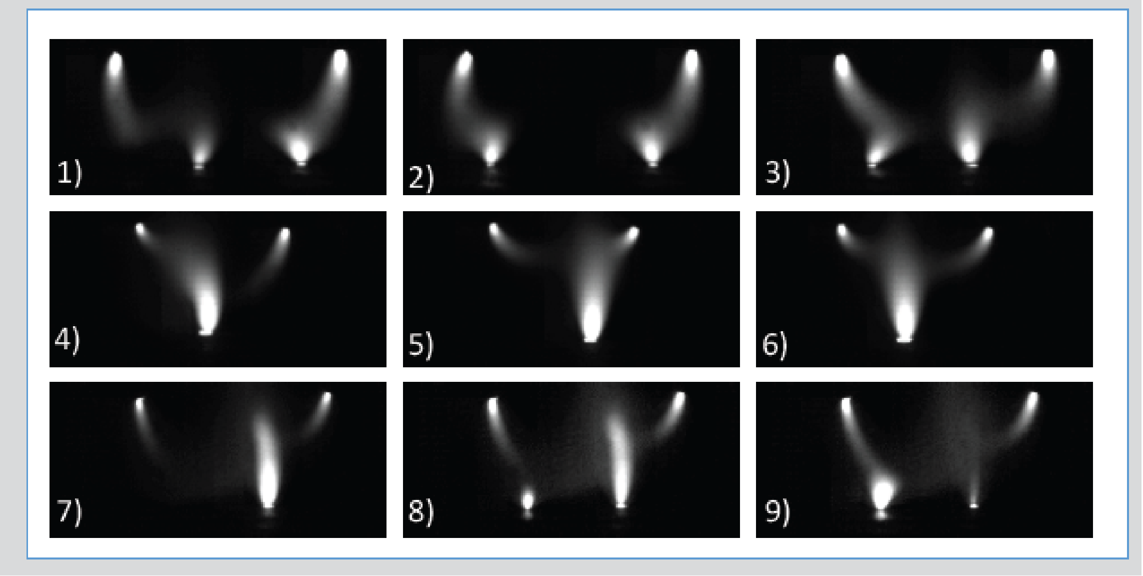

High-speed imaging of arcs with a cathode-anode distance of 25 mm.
1,2,3 show non consecutive frames of separate arcs.
4,5,6 show non consecutive frames of merged arcs.
7,8,9 show consecutive frames of a jumping arc.

Predictor vs. predictor scatter plot. It is desired to find predictors that cluster the data of the same category.

In this case, the "No arc" mode is well clustered.

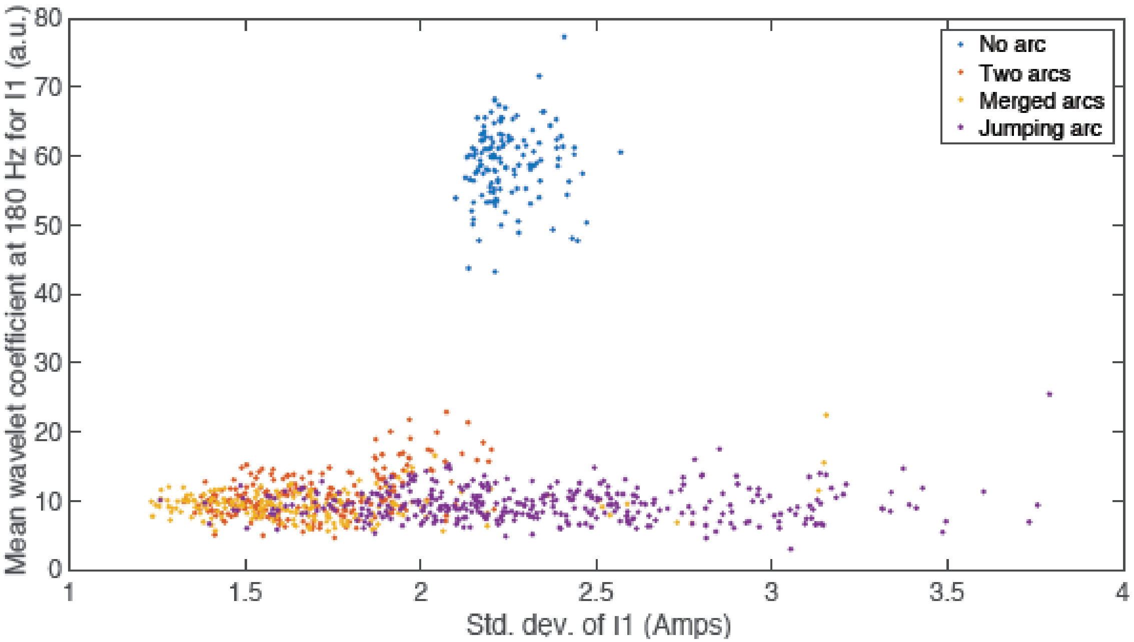

D. Burkat, Canada

High-speed imaging and electrical diagnostics of interacting arcs in dual cathode electric arc furnace

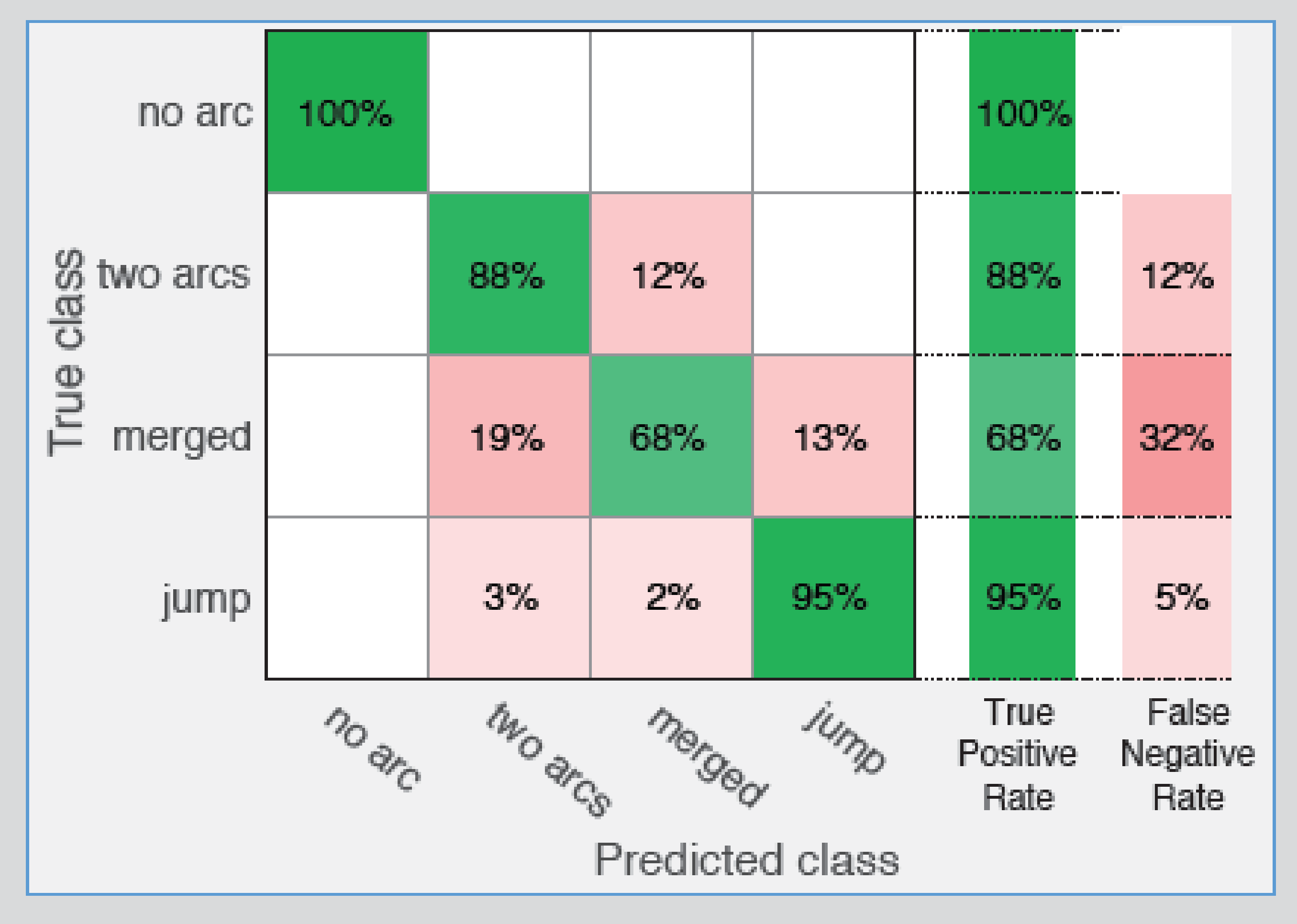

Results:

Arc is elongated, partial merging arcs at anode occurs. 4 arcs observed with different structures that can be differentiated by (V,I) characteristics. Validation of the model obtained with the weighted k-nearest neighbors algorithm: 75% (688 windows) of the data was used to train the model and 25% (229 windows) of the data was used to check the performance. Correct predictions are located along the diagonal.

Peter Ondac, IPP, Rep tcheque

Experimental investigation of plasma in arc-anode area

PRES disponible

Objectives : DC torch anode attachment : lifetime of the anode, stability of the flow, movement of the anode attachment in restrike modes

Studies: Anode surface under different experimental conditions, Movement on the surface and anode attachment area

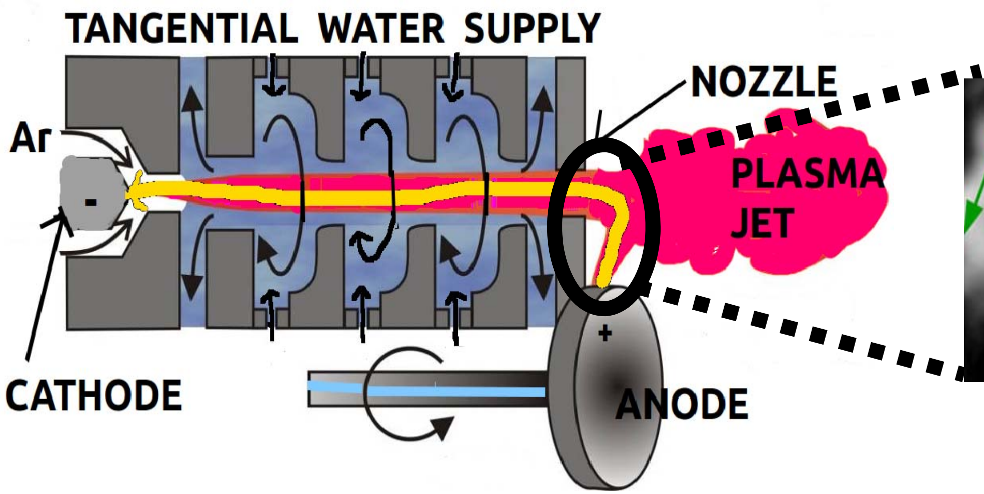

Exposure time: 0.29 µs

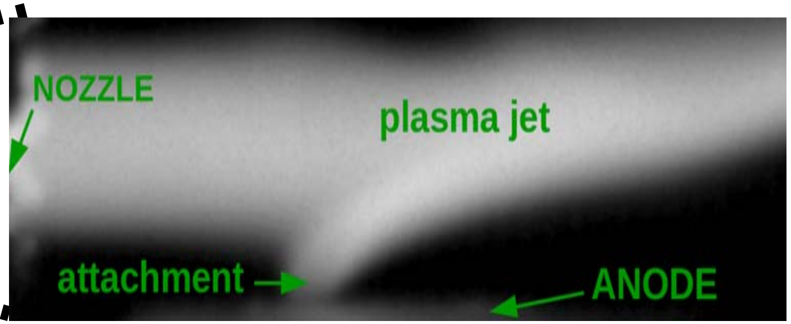

gray filter (1000x) / monochromatic camera picture

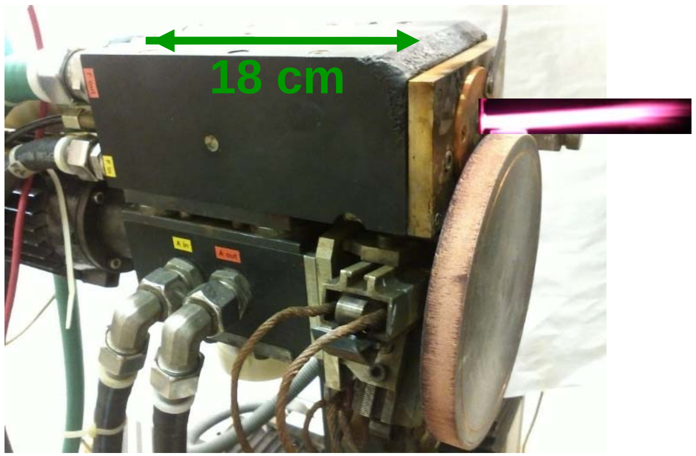

High-speed camera
1.080.000 fps/min, texpo=0.25micros
Synchronized cathode-anode voltage (rate 80MHz)
Arc Current (300 – 600 A), Arc Voltage (230 – 310 V)
Power (70 – 185 kW), Plasma Tmax 25kK
Ar (6 – 40 slm), Water (18 g/min)

Experiments : Observation of the movement attachment during the restrike

Development - determination of plasma effective electrical conductivity

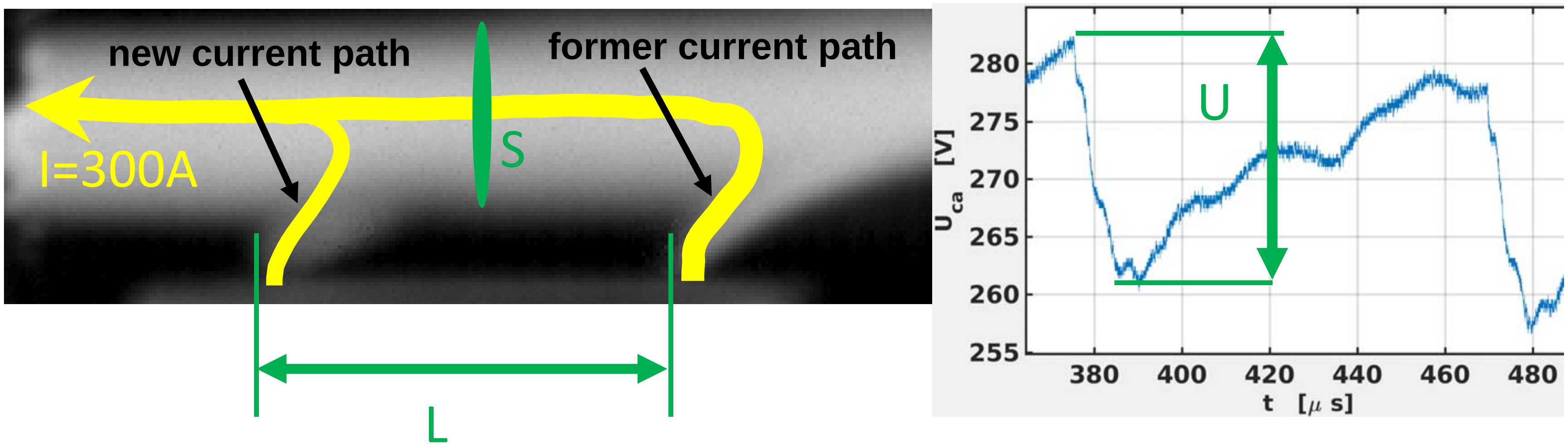

effective electrical conductivity of plasma:

$$\sigma = \frac{I \cdot L}{U \cdot S}$$

$\bar{I} = 300\,A$ $\quad \bar{U} = 18\,V$

$\bar{L} = 10\,mm$ $\quad \bar{S} = 20\,mm^2$

mean(σ) = $9\cdot10^3$ $(\Omega\cdot m)^{-1}$

corresponding effective temperature 500 K (in agreement with spectroscopy measurements)

u(σ) = $4\cdot10^3$ $(\Omega\cdot m)^{-1}$

standard uncertainty

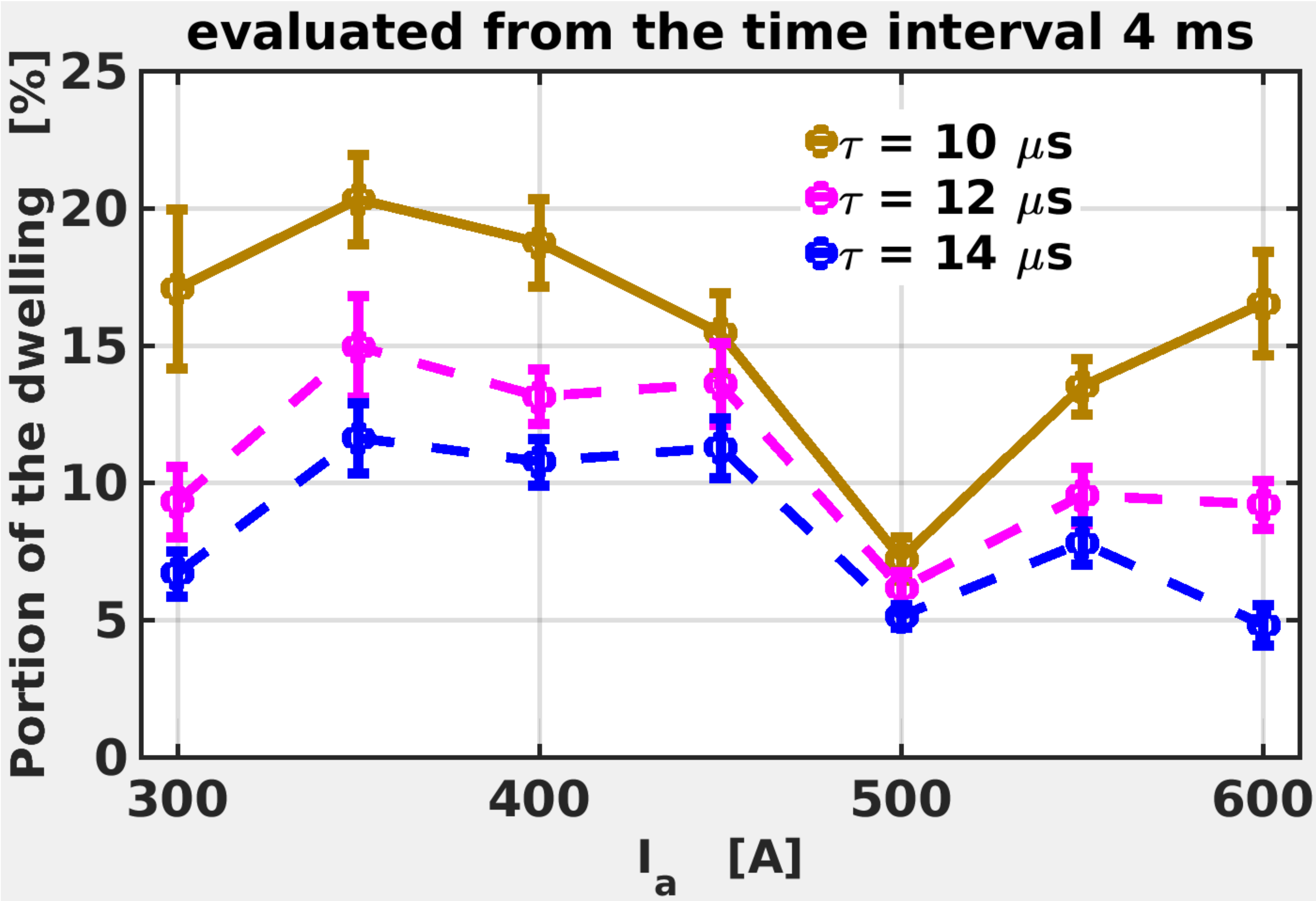

Regarding the craters creation on the anode surface, I=500A is the most optimal.

Results :

- Periodic movement along the anode surface

- The attachment often suddenly slows down (dwells) and makes craters on anode surface. These stops are located at inhomogeneities with higher evaporation

- The reattachment process is related to plasma electrical conductivity.

- They developed a method of determination of plasma effective electrical conductivity.

- They investigate creation of craters on the anode surface by observing the dwelling of the attachment. Irregular wearing surface of the anode

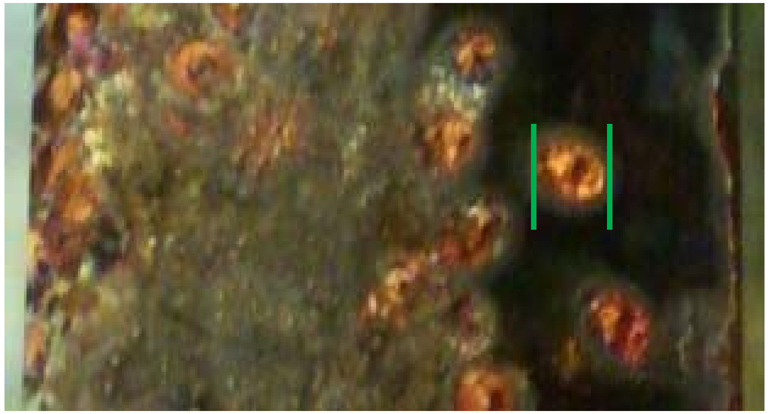

Anode surface after 30 min

crater; ≈0.5 mm

PRES disponible

Study : decrease the electrode erosion by forcing the arc attachment to move in the azimutal direction

How: either by imposing an axial B or by rotating gas flow.

Tools: plasma torch

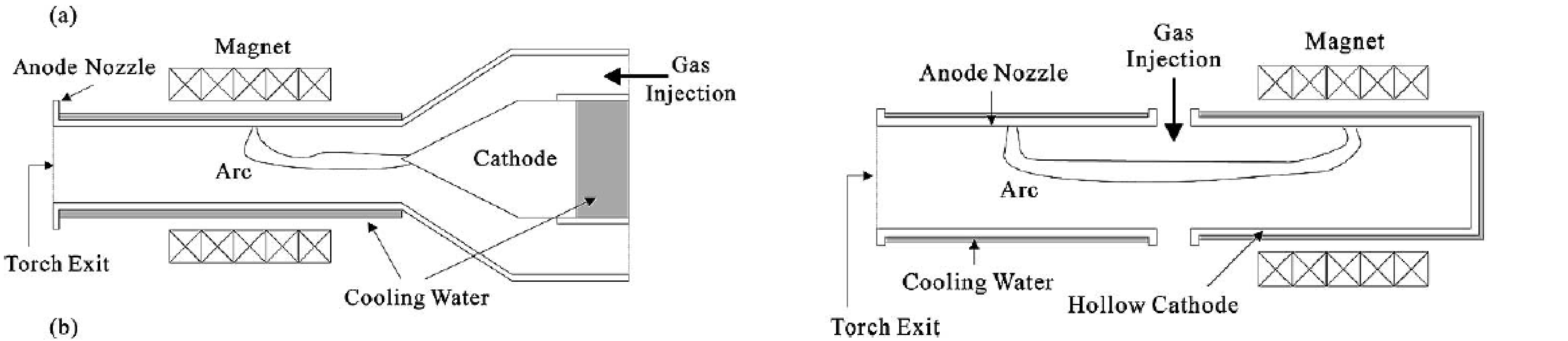

The arc is forced to rotate in order to spread the heat load.

Azimuthal motion of arc is caused by axial magnetic field.

Valerian Nemchinsky, USA

Axial motion of magnetically driven rotating arc

<u>**New solution :**</u> one or few current carrying cables located along the axis outside the concentric arc electrodes. Production by the cables of a tangential B in the inter-electrode gap (different directions at different azimutal angles). Interaction between B and radial arc current induces oscillation and slow drift in the axial direction spreading the thermal and erosion load.

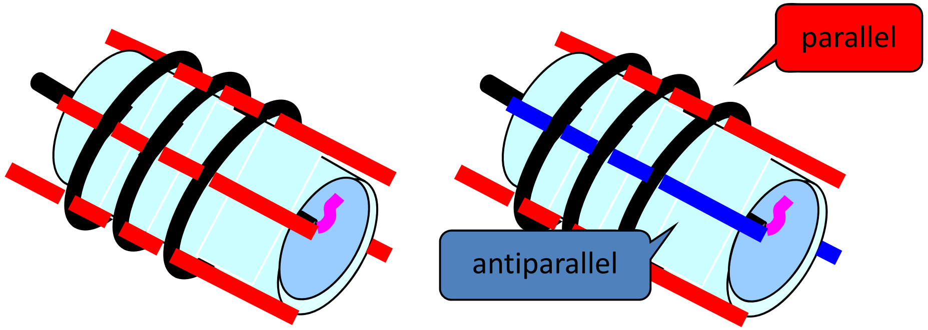

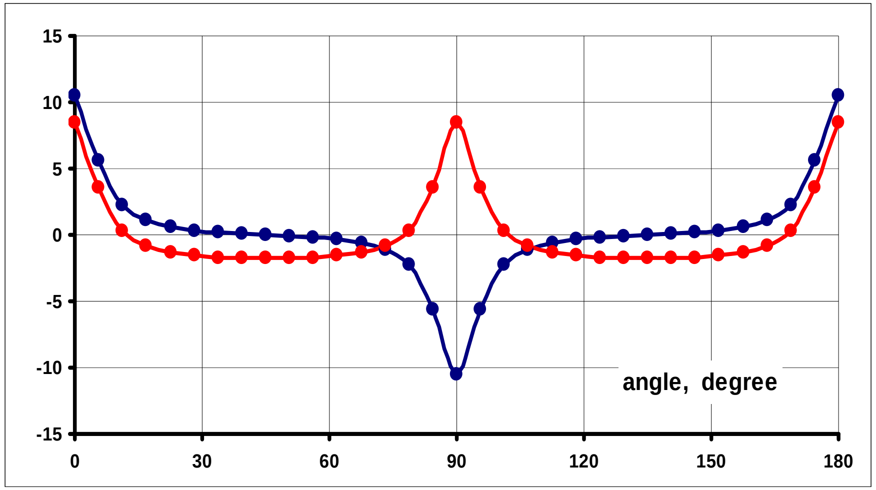

Red and **Blue** are cables creating azimuthal magnetic field (parallel, antiparallel connection)

In addition to a standard method of spreading the heat load to arc electrodes by forcing the arc to rotate, a method is suggested for further spreading the thermal load. By a special arrangement of cables outside the torch, the arc is forced to oscillate and drift in axial direction.

Axial drift of the oscillations maxima as a function of the total rotated angle.

A stable axial motion is established after some initial period

Four parallel cables

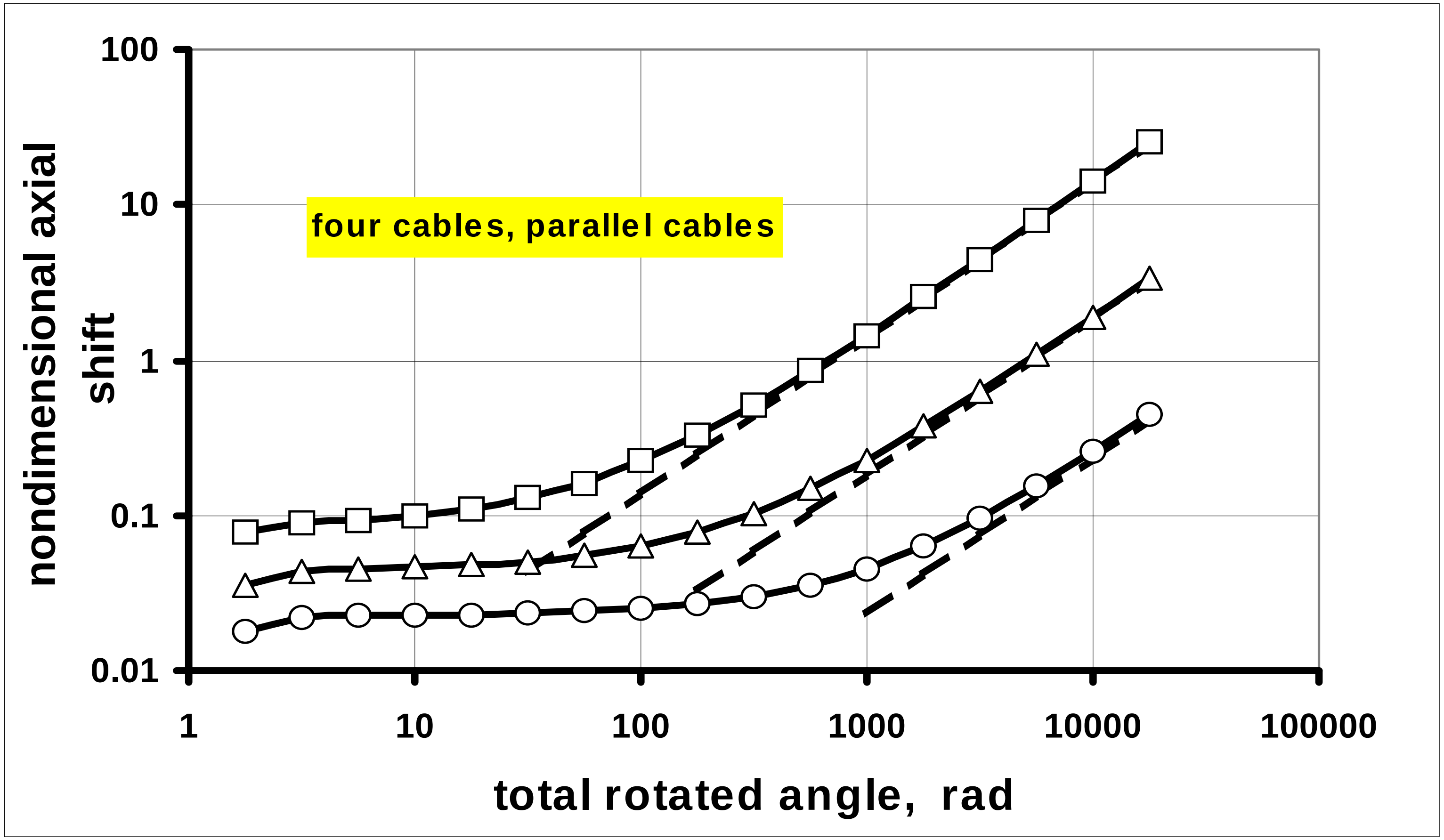

Valerian Nemchinsky, USA

Axial motion of magnetically driven rotating arc

In addition to a standard method of spreading the heat load to arc electrodes by forcing the arc to rotate, a method is suggested for further spreading the thermal load. **By a special arrangement of cables outside the torch**, the arc is forced to oscillate and drift in axial direction.

The direction of this drift can be **reversed by changing the direction of current/currents in the cable/cables** creating the magnetic field. Periodic changing of this direction would expand the arc trajectory into a band. The width of this band could be controlled.

The analysis was performed for arc rotation caused by an axial magnetic field. It is not necessary to have an axial magnetic field to force the arc to rotate. **It could be done by a gas vortex also**. The suggested method should work in this case as well.

Xiuquan Cao, Chengdu Sichuan china

Study on the ignition process of plasma torch

Study : Non-transferred DC arc plasma torches with segmented anode

State: few studies with segmented anode

Theory: analyze of the ignition process

Experiments: analyze of ignition for different ignition parameters

Comparison: successful ignition by optimisating the ignition parameters and the DC power source

TIG WELDING

Hiroki Takahashi, Tokyo, jappan
Distribution of an ar arc contaminated with nitrogen in pulsed TIG welding

Study : Arc welding pulsed TIG

State:
Welding defects occurs due to high currents
Few studies with N2

Study :
Calculation with EMTP (ElectroMagnetic Transients Program) simulation at peak current
Distribution Argon arc with N2 and prevent melting depth
N2 concentration , radial flow velocity, arc temperature

Results:
Concentration N2 becomes low into the arc, low near the anode
Electrical radius becomes small leading to an increase of the radial flow velocity
Diffusion coefficient decreases with temperature over 5000K

Isabelle Choquet, Sweden
A physical based model for thermal plasma arc attachment on a W-ThO2 cathode

Study : Arc attachment, cathode-arc coupling W-ThO2 cathode
State: Contradictory assumptions in the literature, modelling must be simplified
Goal : the physical structure of the cathode must be taken into account in the modelling to better consider the arc attachment

Experiments: **A**rc 5mm, sharp cathode geometry
Theory : model of cathode layer, partial LTE, space charge layer, Knudsen layer, ionization layer, plasma in LTE

Result :
* Space charge emitted electrons is negligible
* Richardson-Dushman emission + Schottky correction must be used if Thorium doped tungsten cathode
* Caracterized by thermoionic emission regime
* Radiative heat absorption from plasma at surface is not negligible compared to radiative emission
* If non-homogeneous structure and composition of the cathode is not taken into account : over estimation of the extent of the arc attachment, and under-estimation of Tarc

The physical strucuture (inhomogeneity) of the cathode must be taken into account.
influence on temperature, pressure, arc attachment

Yoshifumi Maeda, Japon

Heat transfer decrement affected by lateral gas flow velocity in tig arc welding

Application: TIG welding

State: Arc deflects to leeward side when lateral gas flow velocity increases too much, because heat transfer decreases. Heat conduction and electron inflow are dominant in Heat transfer to the anode **BUT** Heat conduction decreases to anode because of arc T° circumference is cooled by lateral gas near anode. Central part J increases because of the I section decreases and electron inflow increases

Study : why heat transfer decreases when lateral gas flow velocity increases?

Tools : EMTF (Electrical Magnetic Thermal Fluid) simulation

Results : Heat conduction decreaes due to the decrease of the heat conduction

Others

Aurelie Bellemans, Belgium

Reduction of a collisionnal radiative argon model comparing a modified binning method with principal component analysis

PRES disponible

State: to reduce the complexity of reactive models, too many species, complex chemical reactions, different time-scale, often 0D or 1D

Different reduction techniques: limit the number of species, time-scale reduction (rate-controlled, singular perturbation for combustion), coarse-gain models (binning methods used of rovibrationnal nitrogen chemistry)

This work : 34 species reduced collisional radiative argon model, two techniques

Detailed chemistry ⟶ Reduced physical models

Technical objectives:

1. Study of system dynamics
2. Development of the reduced model
3. Step-to-step model verification and validation

Aurelie Bellemans, Belgium
Reduction of a collisionnal radiative argon model comparing a modified binning method with principal component analysis

Two techniques

(1) modified binning method:
Excited states are separated from the ground state,
Average through a Maxwell-Boltzamnn distribution
Extra energy equation is solved for regrouped states

(2) Principal Component Analysis (PCA):
Reducing of the number of variables
Projection on a base of principal components, covariance matrix
The advantage lies in the conservation of detailed chemistry information for every species (lost in binning method).

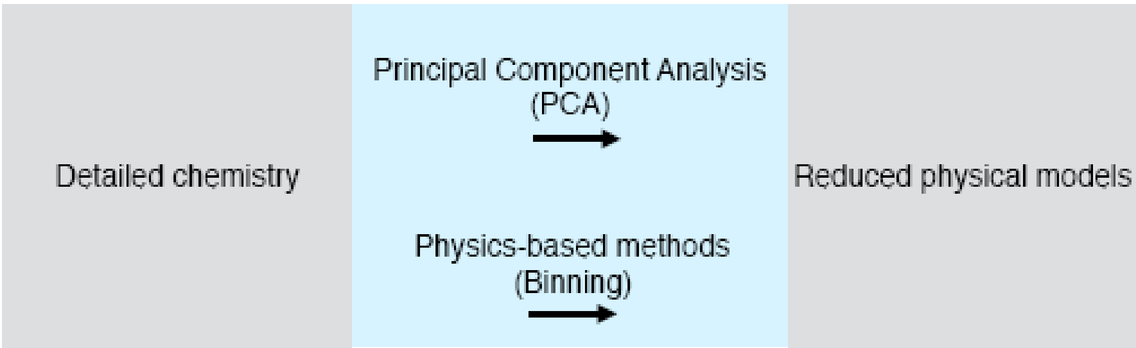

Principal Component Analysis (PCA) reduces the system

Full model:

Pre-processing:
Centering & Scaling

↓

Eigenvalue problem on covariance matrix :
eigenvectors = principal components

$$S = \frac{1}{n-1} X^T X = ALA$$

↓

Select most important PC's (q)

↓

Reduced model:

Project data on PC's:

$$Z_q = XA_q$$

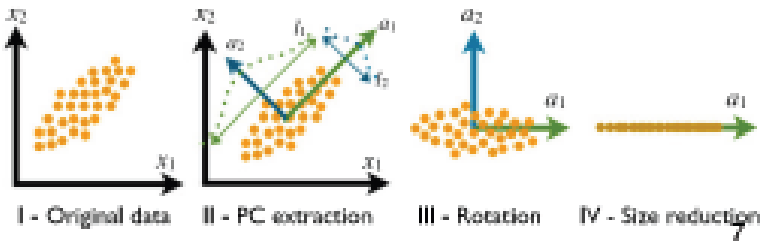

X : $[y_0, \ldots, y_N, T, T_e]$
n : # observations
q : # PC's
Z_q : truncated eigenvectors

Aurelie Bellemans, Belgium

Reduction of a collisionnal radiative argon model comparing a modified binning method with principal component analysis

Local PCA optimises the reduction

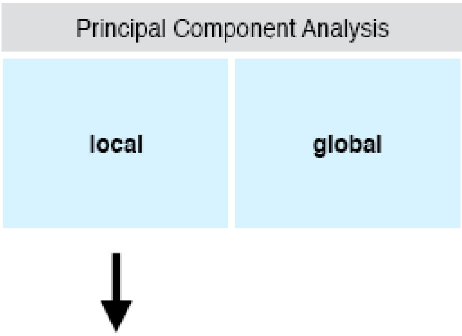

Divide the data in clusters and apply PCA in each of them

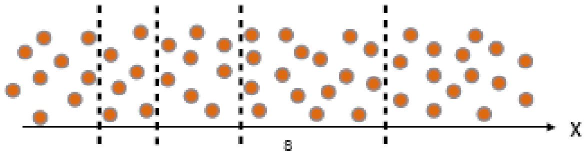

Work :

New clustering algorithm for local PCA

-> simulating re-entry pressure with 6 clusters

-> good reduction for the UTIAS shock tubse cases

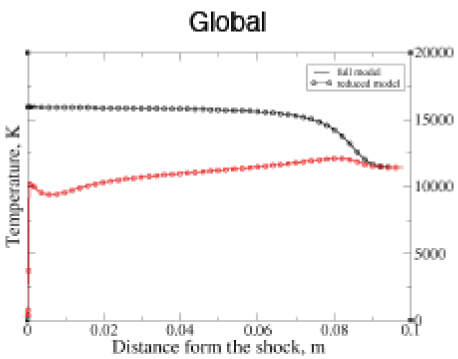

36%

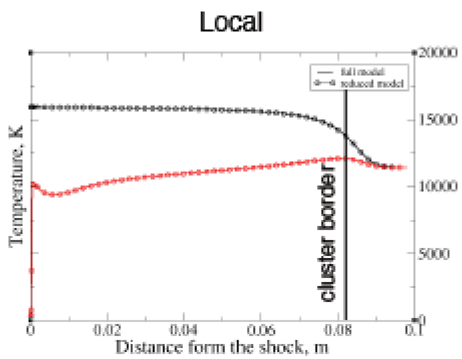

56%

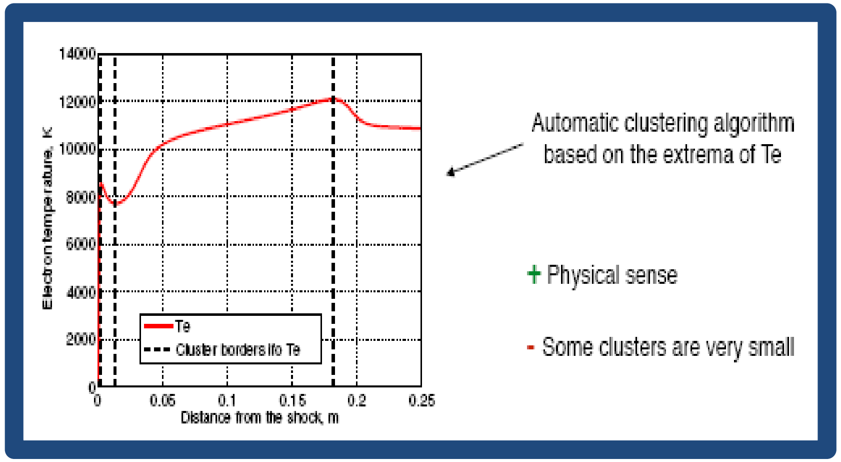

Aurelie Bellemans, Belgium

Reduction of a collisionnal radiative argon model comparing a modified binning method with principal component analysis

Can a modified binning method compete with PCA ?

From 2 temperatures to 3:

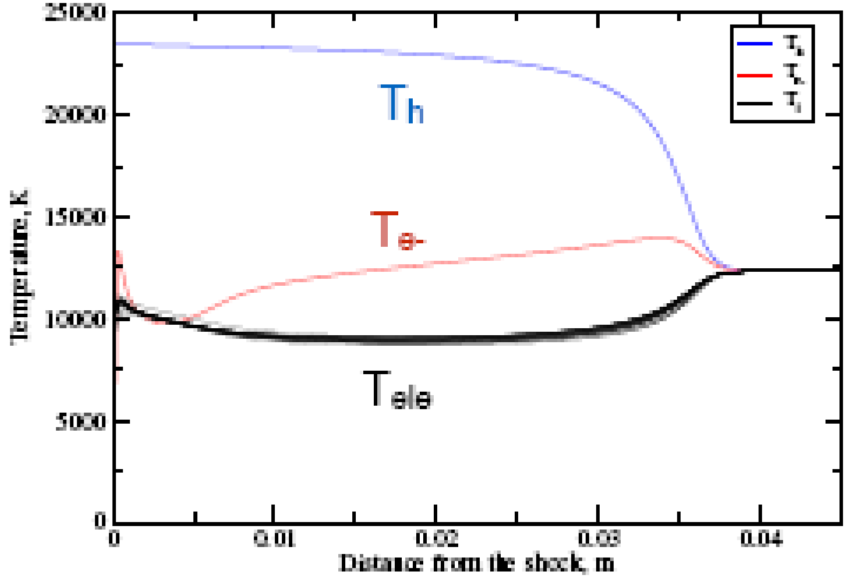

From 34 species to 4:

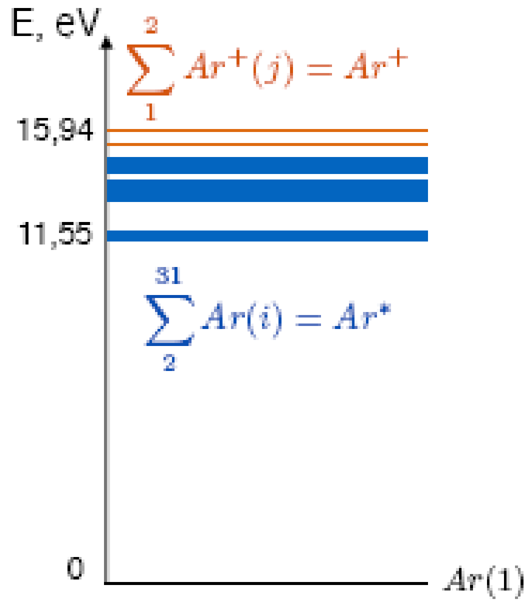

Detailed chemistry is conserved
PCA is capable of reducing radiative systems
47% model reduction for re-entry free-stream conditions
Local PCA has been optimised using the automatic clustering algorithm

Jiri Jenista, IPP, Rep. Tchèque

Investigation of mixing of plasma species in argon-water arc discharge

PRES disponible

Application : production of syngas CO+H2, waste or biomass

Study : numerical simulation of mixing species under extreme temperature and density gradients in arc discharge

Tools : Hybrid Stabilization of electrical arc by axial argon flow and tangential water vortex

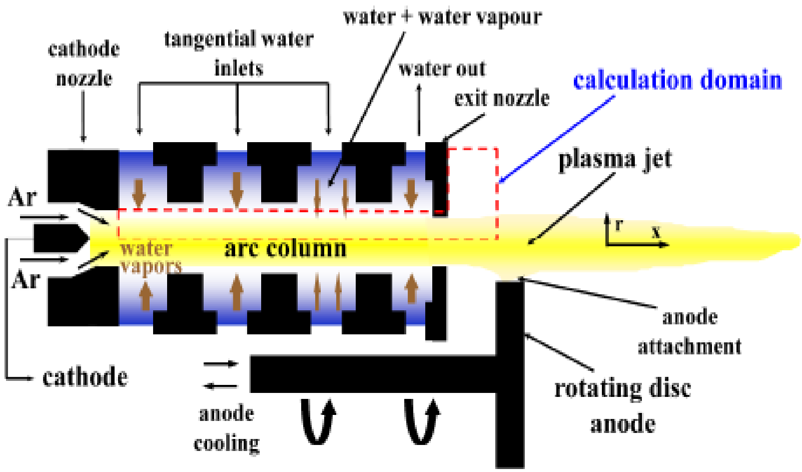

Temp. up to 25 000 K, overpressure up to 1.5 atm.

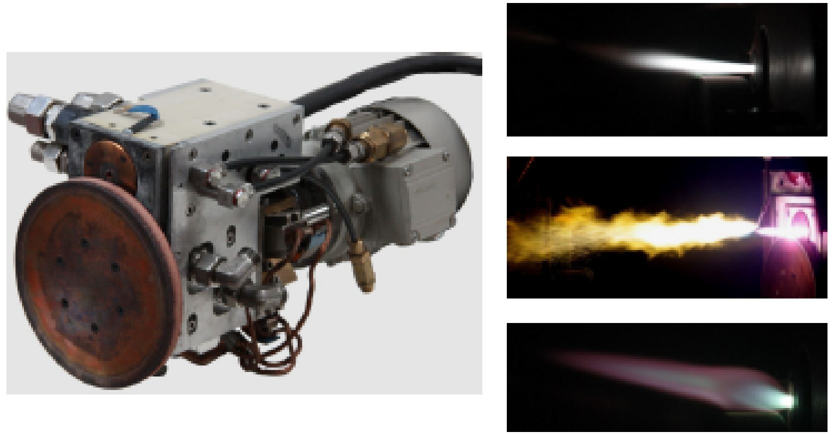

Plasma spraying torch WSP®H 2000 with hybrid stabilization:

Model :

- 150-300A, argon-Water plasma, 12-22.5 slm
- One fluid, 2D, axisymmetric, unsteady, compressible, turbulent flow, LTE
- Oblique structured grid with nonequidistant spacing

38553 Grid points (543 and 71 points in the axial and radial directions)

Equations:

- Mixing inhomogeneous species using combined diffusion coefficients
- Diffusion processes account (due to pressure, T, concentration gradients, E) with gas 1 (argon) and gas B (O2, H2O) – Murphy's concept
- Lorentz force + Radiation losses with partial characteristics method with O2, H2, H2O, OH
- Gravity effects negligible, self-induced magnetif cifeld assumed
- Turbulent effects treated by Large Eddy Simulation (LES) with Smagorinsky subgrid-scale model (Smagorinsky coefficient Cs=0.1, Prandtl number 0.9)
- Set equations solved by LU-SGS method coupled with Newtonian iterative method
- Roe flux differential method coupled with 3th order MUSCL-TVD scheme
- Electric potential calculated using TDMA algorithm with block correction method

$$500\,K \le T \le 35\,000\,K$$
$$1.0\,atm. \le p \le 3.5\,atm.$$
$$0 \le f_A \le 1.0,\ step = 0.1$$

→

Transport:	Thermodynamic:	Diffusion coeffs.
$\lambda = \lambda(p,T,f_A)$	$\rho = \rho(p,T,f_A)$	$\bar{D}^x_{AB} = \bar{D}^x_{AB}(p,T,f_A)$
$\sigma = \sigma(p,T,f_A)$	$R_g = R_g(p,T,f_A)$	$\bar{D}^T_{AB} = \bar{D}^T_{AB}(p,T,f_A)$
$\eta = \eta(p,T,f_A)$	$c_p = c_p(p,T,f_A)$	$\bar{D}^P_{AB} = \bar{D}^P_{AB}(p,T,f_A)$
	$c_v = c_v(p,T,f_A)$	$\bar{D}^E_{AB} = \bar{D}^E_{AB}(p,T,f_A)$

Jiri Jenista, IPP, Rep. Tchèque

Investigation of mixing of plasma species in argon-water arc discharge

Arc Current effect on the temperature, enthalpy, velocity, pressure, total argon particle flux, argon mass flows, argon mole fraction, enthalpy, combined diffusion coefficients

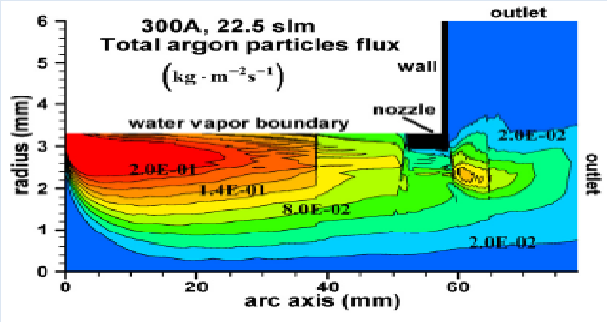

Inhomogeneous mixing of species in the discharge.
Argon are dominant in central regions or the arc
Water are dominant in arc fringes

Combined ordinary diffusion is highest in regions with steep radial temperature
Combined temperature diffusion is highest in a shear layer between argon and water

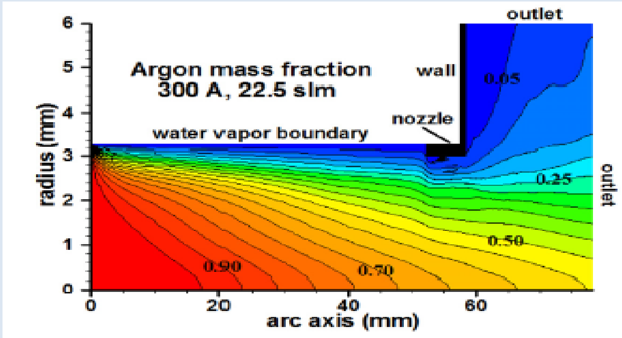

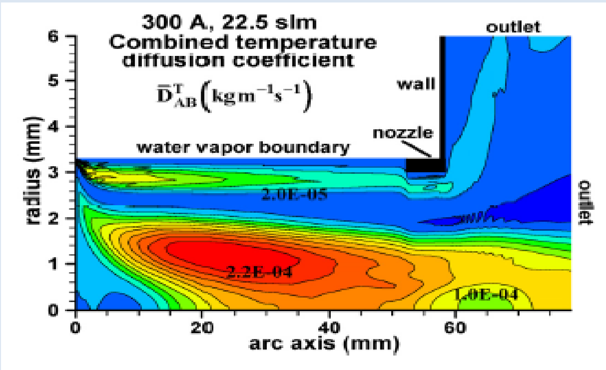

Temperature and ordinary diffusion coefficients are main contributions in the argon mass diffusion flux

PRES disponible

Topic : Plasma spraying of liquid feedstock (suspensions/solutions)

Idea: Basic idea of pulsed plasma spraying with synchronized injection of droplets

Studies:

- Arc fluctuations in conventional DC torch
- pulsed arc regime
- synchronous injection of ceramic ink in pulsed arc jet

Ar-H_2(45-10slm)
400 A

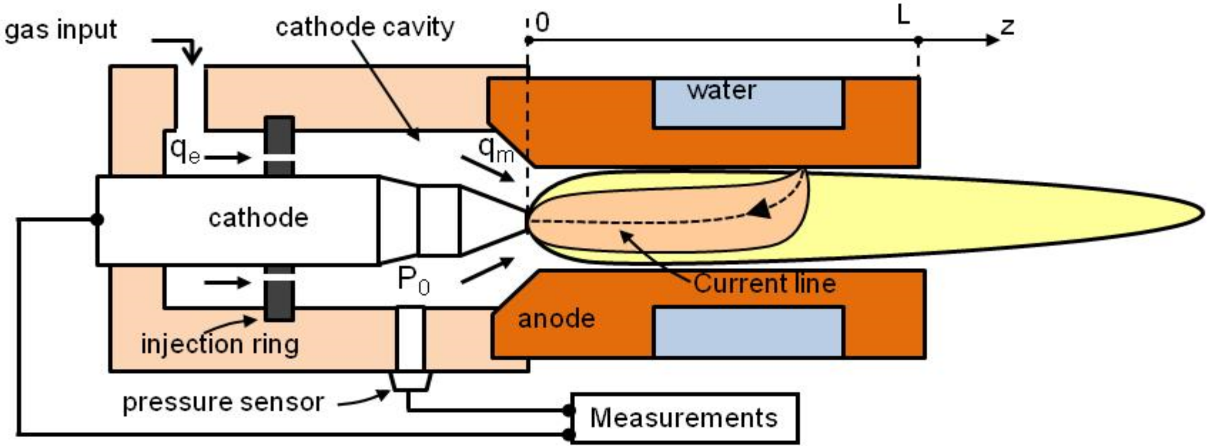

Arc fluctuations in conventional DC torch

Coupling of arc voltage/pressure in DC arc torch

- Filtering voltage
- Filtering pressure
- Helmholtz resonance
- Restrike
- Acoustic resonance

Parameter coupling in a dc plasma torch: simplified model

- *Input parameters*: torch geometry, plasma forming gases, arc current
  Helmholtz arc voltage $v_H(t)$

- *Output parameters*: plasma specific enthalpy and speed
  mass flow rate, **pressure in cathode cavity $P_0(t)$ => $p_H(t)$**

- Energy equation (h, Q_{loss}), momentum equation (u, P_0)
- Mass balance inside the cathode cavity volume V_{cav} (q_m, P_0)
- Properties averaged over the channel cross section at nozzle exit
- Linear approximation

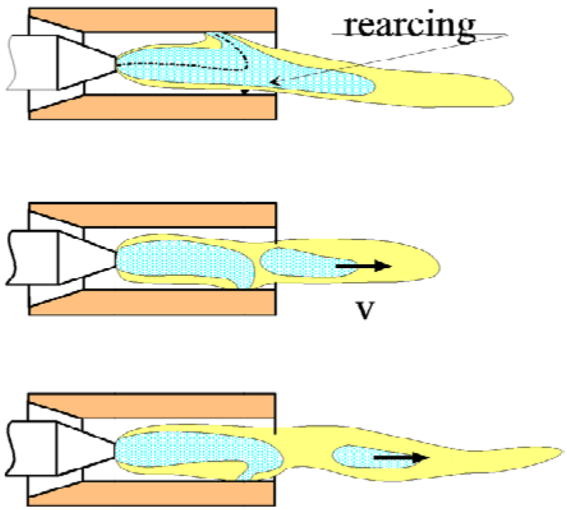

- **Helmholtz mode** – f ~ 4-5 kHz pressure effects-modulation of flow rate
- Restrike mode : rearcing through boundary layer around the column f ~ 10-20 kHz
- Coupling pressure and voltage
- Resonant torch : pulsed arc

Enthalpy modulation : temperature measurements

Arc current frequency 1300 Hz

2 trigger times : $P_{synchro\ 1}$ = 1.2 kW = and $P_{synchro\ 2}$ = 2.1 kW

Exposure time 30 µs + accumulation N_{acc} ~ 50-200

Abel inversion

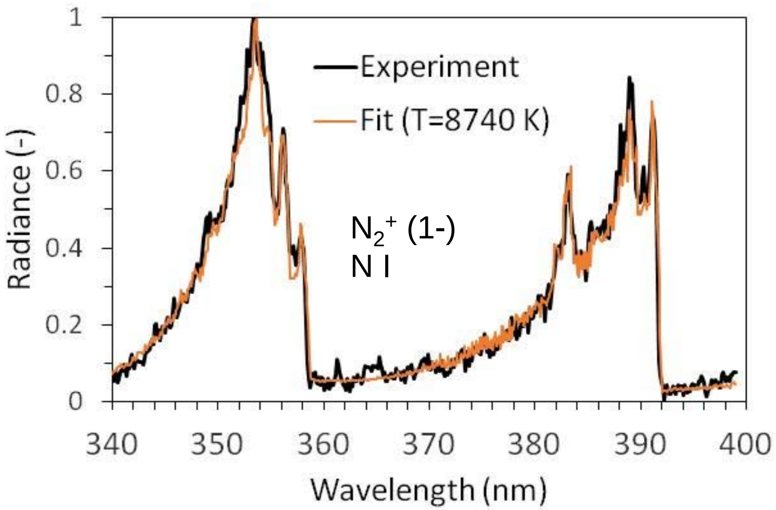

Temperature profile

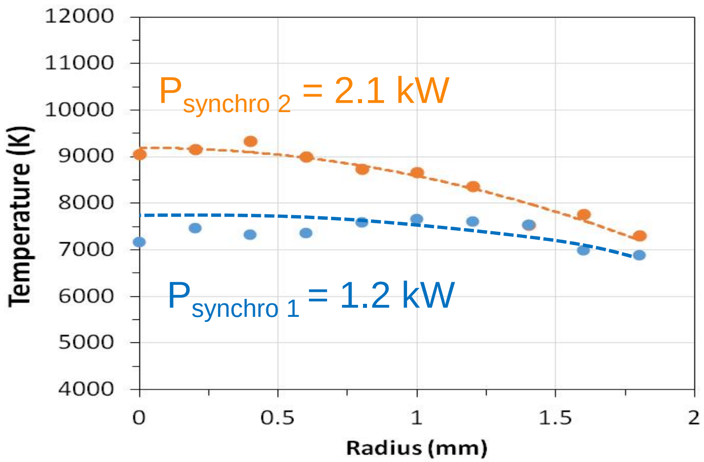

Enthalpy profile

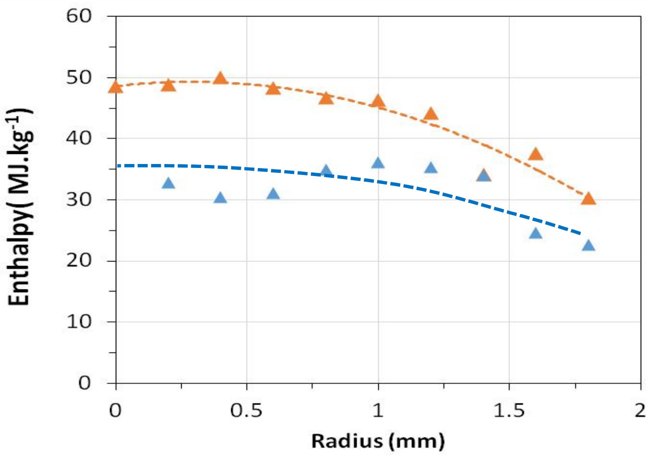

TiO_2 coatings : injection of TiO2 ceramic ink

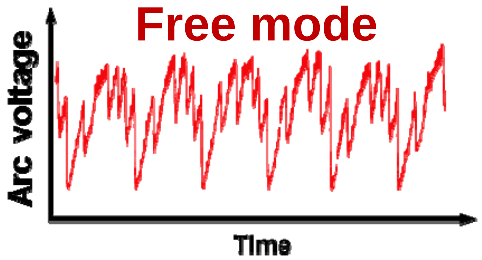

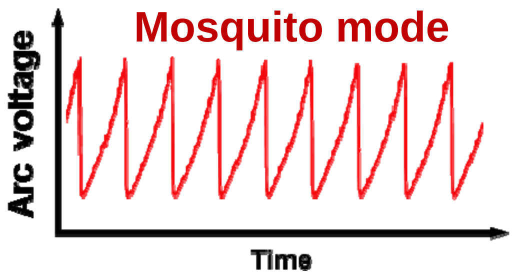

- **Piezoelectric injection :**
  - Aqueous TiO_2 suspension (5vol%, d_{50}=60 nm)
  - Droplet diameter 50 µm, Droplet speed 1 - 3 $m.s^{-1}$
  - Frequency injection = torch frequency = f_0

❖XRD : Rutile phase
❖TEM: cristallised, no amorphous phase
❖Chemical analysis : Ti and O

Without synchronization

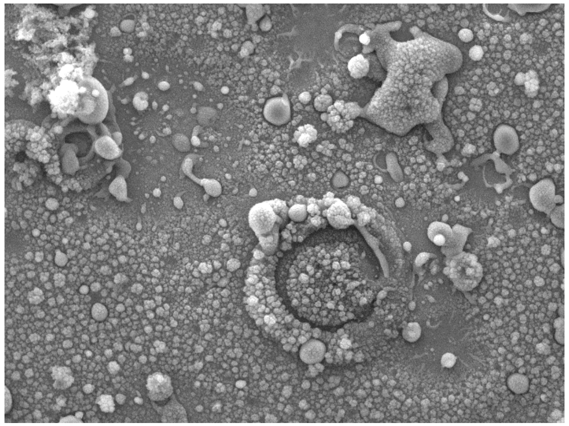

With synchronization

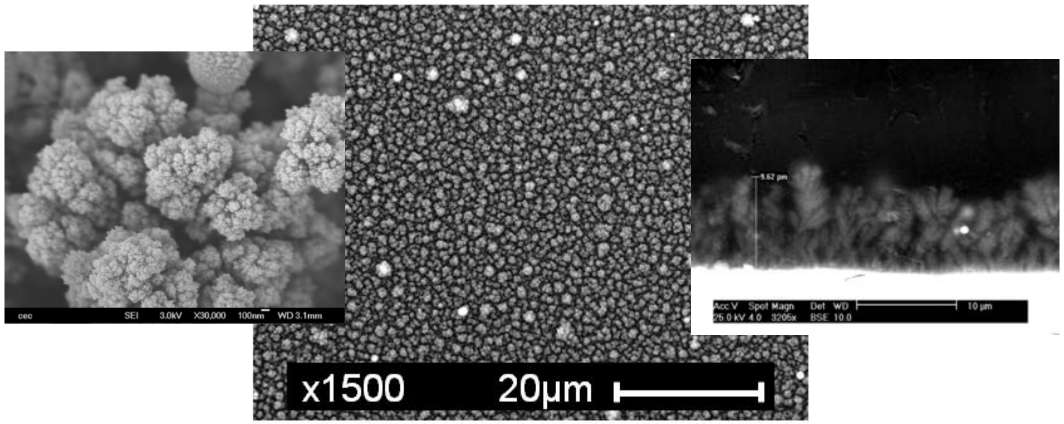

Conclusions

- Controlling the arc instabilities is necessary for nano-sized solid particles:
  - Stabilizing the arc: segmented torches
  - Amplifying the arc instabilities to obtain a pulsed arc jet

- Reproducing in time local plasma/materials interactions provided a synchronous injection of materials is performed

- The modulation of plasma properties affects the momentum and heat transfers from plasma to materials

- Coatings are composed of nanostructures and micro-sized particles

Yann Cressault, Laplace, France

Improvement of Ceramic Halide High Intensity Discharge lamps- study of the UV radiation that could be converted into visible light

PRES disponible

Goals: find new emissive species to replace mercury in lamps

Estimate the UV radiation in order to convert it in visible

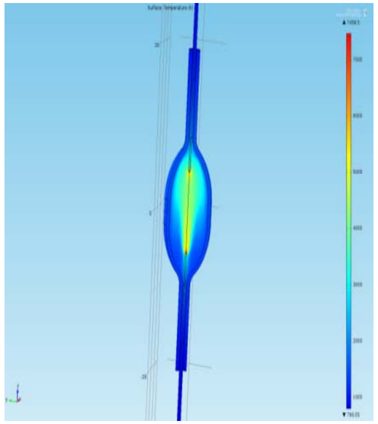

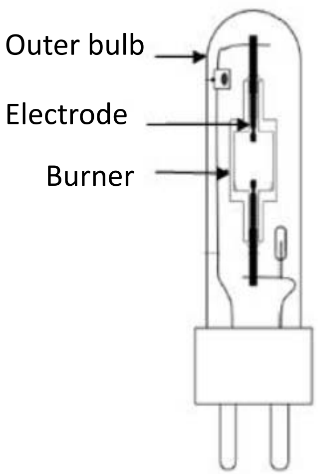

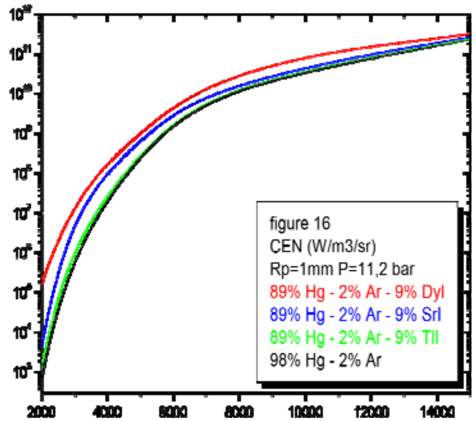

Argon + Mercury

+

Dysprosium

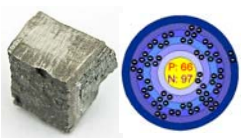

Thallium

Strontium

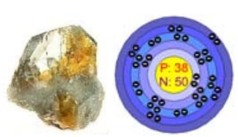

Calcium

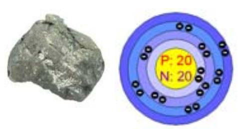

Sodium

Tungsten

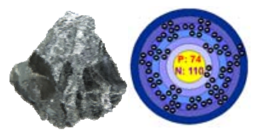

Yann Cressault, Laplace, France
Improvement of Ceramic Halide High Intensity Discharge lamps- study of the UV radiation that could be converted into visible light

Proportion of the power radiated in UV, visible and IR regions, for mixtures at 11.2 bar, 5500K and Rp=1mm

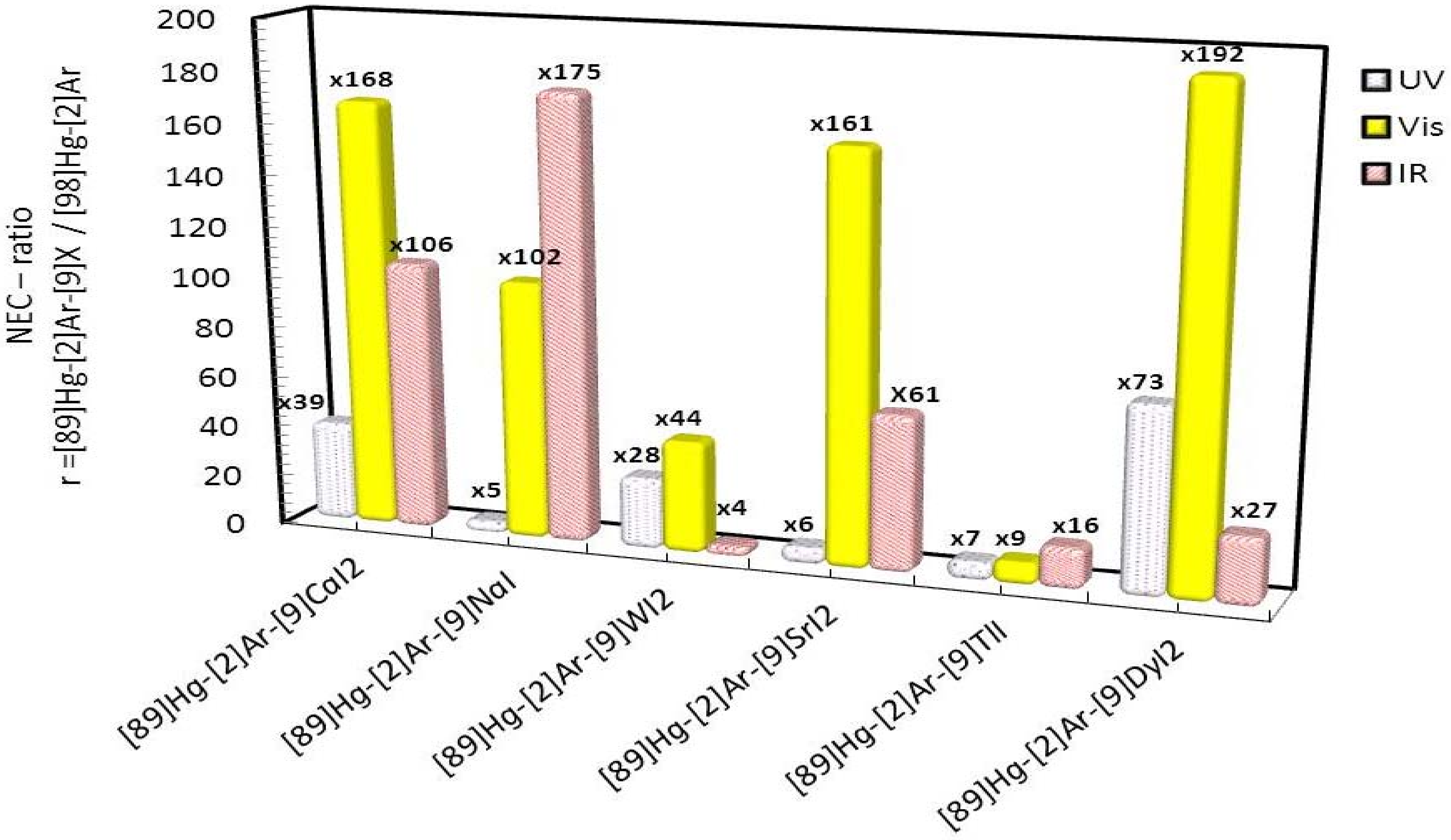

Rohit sharma, India

Thermodynamic properties of hydrogen thermal plasma in local thermodynamic equilibrium

Study : H2, LTE, 5000K-50000K, 1atm, 100atm et 1000atm
Cas 1: Internal Partition Function dependent from Pressure
Cas 2: Internal Partition Function independent from Pressure

Observations:
Differences begin with temperatures increasing with pressure

(1) With pressure dependency
The relationship between compressibility coefficient and ionization degree depends on P
Compressibility and Cp are higher than case (2)

(2) Without pressure dependency
No dependence on P for the relationship between compressibility coefficient and ionization degree
Adiabatic coefficient, isentropic coefficient, sound speed higher in this case

Comparison
The differences increase with pressure for the compressibility coefficient, specific heat and adiabiatic coefficient
The differences are slighter for isentropic coefficient and sound speed.

Qingqing Gao, Xi'an

Composition and dominant species of SF_6/N_2 in a two temperature chemical kinectic model

Application: predict the quentching, breaking attempt

State:

SF_6 is widely used in HVCB, LTE/LCE already studied

SF_6/N_2 substitute SF_6 (N_2 is non toxic, cheaper)

When Ne decreases, energy transfer between electron and heavy particles is not sufficient

2T modelling is necessary

LTE/LCE already studied

Study :

2T chemical kinetic model

Thermal and chemical departures from equilibrium

P=4atm, 12000K->300K, Teta=Te/Th=f(Ne)

T* is introduce to determine the chemical constant rates, smooth transition from Th to Te.

Results: the dominant species are determined within different temperature ranges

Charlotte Boukandou-Mombo, Canada
Time-dependent collisional radiative model for helium

Study : Helium discharge subjected to fast varying-excitation source, fully time-dependent
Model : powerfull nanosecond excitation source
- 0D collision radiative model (CRM), Bolzmann equation for electron kinetics
- Set of rate equations for 31 energy levels atomic He, molecular ions, eximers (ionization, recombination, excitation, superelastic and elastic collisions, effective ambipolar diffusion...), radiation trapping and self-consistent gas temperature calculation
- New: large number of processes, species, fully time-dependent way for solving electron Boltzmann Equation

Results : plasma is strongly out of Equilibrium, specific properties

Seisui Ono, Japon

Arc conductance and flow velocity affected by wall radius of wall-stabilized arc

Study : prevent the breakdown (re-ignition and thermal reignition after arc interruption)

State : GCB must have more reliability, improvement of the arc interruption of abnormal fault current. Stable supply of electric power is indispensable.

How: by decreasing the arc conductance which depends on the arc T° distribution and arc volume

Study: arc conductance and flow velocity affected by wall radius of wall stabilized arc. Flow rate and T° distribution calculated by changing the wall radius. Arc conductance calculated

Results: If wall radius decreases, axial flow velocity increases, arc T° and arc conductance decrease.

Simone Bianconi, Italie
Design oriented modelling for the synthesis of copper nanoparticles by a radio-frequency induction thermal plasma

RF-ICP Torch for nanoparticles production
+ High energy density, chemical reactivity, process purity, large volume, long residence time of precursors, high cooling rate (10^4/10^5 K/s)
- expensive cost
* Study :
modelling in order to optimize the design of RF-ICP synthesis process of Cu nanoparticles starting from a solid precursors
effect of geometry reaction chamber
effect of quentoching strategy (injection of gas effects to flow fields, T°, cooling rates, particles deposition on walls which must be decreased)
* Tools :
thermo-fluid dynamics, with electromagnetic fields
including precursor trajectories, thermal history, nanoparticles nucleation/growth, radiative losses from Cu vapour and effects on evaporation of precursors

Hybrid systems

Koichi Yasuoka, Japon
Arc-less commutation in hybrid DC circuit breaker

PRES disponible

Application : DC circuit breaker for DC power transmission (DCCB)

Process : electrical contacts move, contact resistance increases, voltage change, temperature of contact surface increases, melting point, arc discharge is ignited.

Hybrid DC : electrical contacts + semiconductors + metal-oxide varistor (MOV)
small contact resistance, fast interruption, arc-less commutation

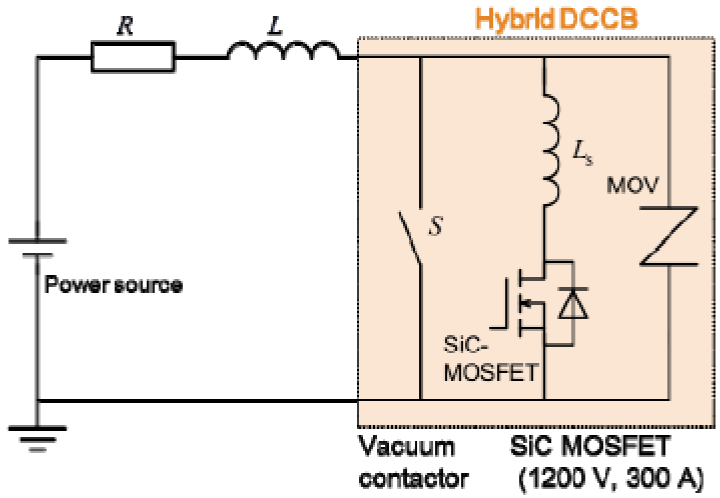

Basic operation of the DCCB

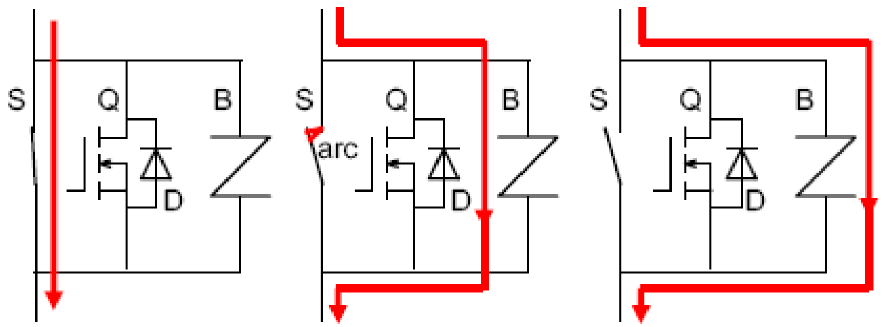

Use of the molten metal-bridge voltage at the opening stage of the contacts.
The magnitude of the molten-bridge voltage is just enough to turn on SiC-MOSFET devices under specific conditions.

Koichi Yasuoka, Japon
Arc-less commutation in hybrid DC circuit breaker

VI waveforms during opening sequence

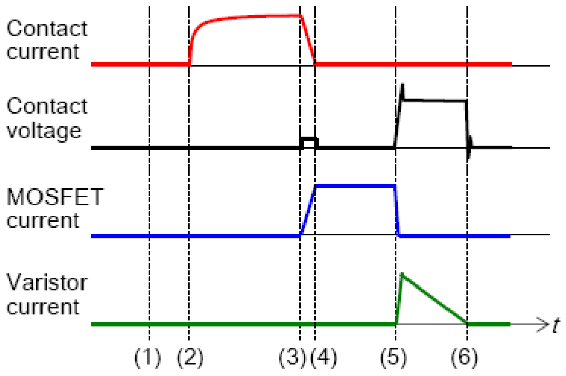

Voltage at the contact with arc discharges

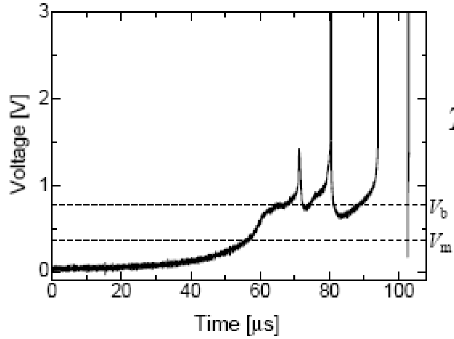

$$T_{max} = \sqrt{\frac{V_c^{\,2}}{4L} + T_0^{\,2}}$$

Arc less commutation of DC 76 A with two SiC-MOSFETs

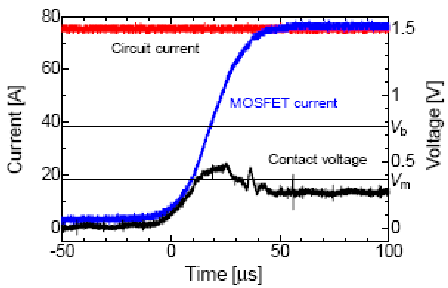

Voltage and current waveforms at a circuit current of 76 A with two SiC-MOSFETs connected in parallel. Arc less commutation was achieved.

Arc generation during interruption of 140 A

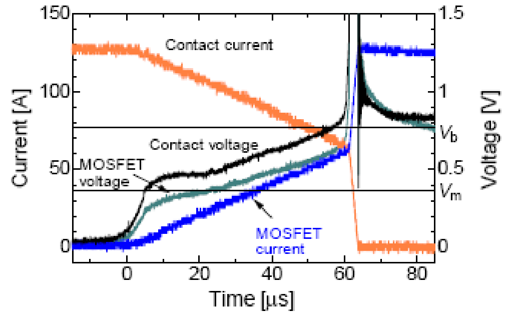

Voltage and current waveforms at a circuit current of 140 A with four SiC-MOSFETs connected in parallel. An arc discharge was initiated after 60 ms within a duration of 3 ms.

Arc less commutation of DC 140 A with four SiC-MOSFETs

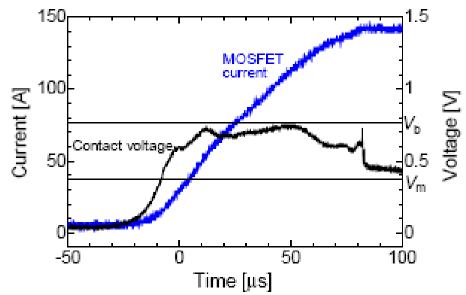

Voltage and current waveforms at circuit current of 140 A with four SiC-MOSFETs connected in parallel. Arcless commutation was achieved.

Solution : SIC-Mosfet power devices with 4 parallel SiC-Mosfet. Arcless commutation of DC current was observed with a Ag-W vacuum contact and SiC-MOSFETs at current values of ^{2}78~140 A.

43rd IEEE International Conference on Plasma Science,
June 19-23, 2016

Merci à l'AAE